Lithium Production and Soft X-ray Emission in Neutron Star Soft X-Ray Transients Cen X-4 and Aql X-1

Shin-ichiro Fujimoto[1], Ryuichi Matsuba[2] and Kenzo ARAI[3]

[1)] *Department of Control and Information System Engineering, Kumamoto National College of Technology, Koshi, Kumamoto 861-1102*

[2)] *Institute for e-Learning Development, Kumamoto University, Kumamoto 860-8555*

[3)] *Department of Physics, Kumamoto University, Kumamoto 860-8555*

(Received September 30, 2010)

We investigate production of Li in soft X-ray transients (NSSXTs) during quiescence. Lithium is abundantly synthesized in a hot accretion flow and is transfered to the surface of a secondary star. Almost all charged nuclei in the accretion flow are outflowed by the magneto-centrifugal forces, so that the accretion flow is mainly composed of neutrons. Accretion energies of neutrons liberated on the surface of the neutron star naturally explain the origin of blackbody-like soft X-rays from a quiescent NSSXT. It is found that for reasonable values of the mass accretion rate $\dot{M} = 2-4\times10^{-11} M_\odot\ \mathrm{yr}^{-1}$ from the secondary and the magnetic field $B_{\rm NS} = 2-3\times10^8$ G of the neutron star, the abundance of Li on the secondary is LI/H$\simeq 10^{-9}$ and the soft X-ray luminosity is $L_X = 2-3\times10^{32}\,\mathrm{erg\,s}^{-1}$, which are comparable to the observed values in Cen X-4 during quiescence. Moreover, the isotopic ratio ^{6}Li/ ^{7}Li is found to be comparable to the observed value. The scenario for the Li production and the emission mechanism of the soft X-ray in terms of neutron accretion explains the non-detection of Li in Aql X-1 due to strong magnetic fields. These facts strongly suggest the existence of a hot accretion flow in an NSSXT during quiescence.

§1. Introduction

High abundances of Li have been observed in late-type secondaries of black hole soft X-ray transients (BHSXTs) and a neutron star soft X-ray transient (NSSXT) during quiescence,[1)] though Li is likely to be destroyed in the deep convective envelope of a late-type star. The Li enrichment has not, however, been observed in a late-type secondary of a compact binary with a white dwarf.[2)] These facts strongly suggest that Li is produced in BHSXTs and NSSXTs[3),4)] and that the nature of the primaries is crucial for the production mechanism. Recently, Li production has been examined[5)] on the surface of the secondary in a BHSXT through spallation of CNO nuclei by neutrons from a hot accretion flow. The evaluated abundances of Li has shown to be in good agreement with observed abundances of seven BHSXTs for updated binary parameters, cross sections of neutron-induced spallation reactions, and mass accretion rates derived from the spectrum fitting of multi-wavelength observations of the quiescent BHSXTs.

However, the Li production is not enough in NSSXTs because of low accretion rates corresponding to low X-ray luminosities. The Li enhancement on the secondary is suggested[3)] in terms of the transportation by magneto-centrifugal forces through propeller effects of Li synthesized by α-α reactions in an advection domi-

nated accretion flow (ADAF) around a neutron star. Since timescale for deposition is much shorter than that for the convective Li burning, we should take account of Li deposition from the secondary via mass accretion onto the neutron star.

Moreover, X-ray emission from NSSXTs in quiescence is fitted with blackbody-like soft and power-law hard components. Although the origin of the hard component is still unclear, the energy source of the soft X-ray is considered to be residual polar accretion onto a neutron star from ADAF.[6),7)] Even when the propeller effects operate, accretion through the polar region of the star is possible because of weak centrifugal forces in the region. The fraction of the mass accretion rate that reaches the neutron star surface has been estimated to be 10^{-3}, which could be much lower if the accretion flow has a toroidal morphology with empty funnels along the rotational axis.[7)] We note that MHD simulations of ADAF show that the flow has funnels with densities lower than that at the equatorial plane.[8)]

As magnetic fields of the neutron star have no influence on neutrons produced in ADAF, neutrons can accrete onto the neutron star even after the propeller effects operate. Consequently, the accretion flow near the neutron star consists of neutrons only. Gravitational energy of neutrons is liberated on the surface of the star. This is a possible energy budget to the soft X-rays from NSSXTs.

In the present study, we examine the production of Li through the transportation of Li from ADAF to the secondary, taking into account the Li deposition from the surface via the accretion. We propose a new mechanism to produce soft X-rays from NSSXTs through the liberation of the gravitational energy of neutrons on the surface of the star.

§2. Abundance distribution in an advection dominated accretion flow around a neutron star

We consider ADAF around a neutron star of mass $M = 1.4M_\odot$. Temperature of ions is given by[9)]

$$T = 3.7 \times 10^{12} \frac{r_{\rm in}}{r}\ {\rm K} = 31.9 \frac{r_{\rm in}}{r}\ {\rm MeV}. \tag{2.1}$$

Here $r_{\rm in} = 3r_g$ is the radius at the inner edge of ADAF, where r_g is the Schwarzschild radius. Number density of gas is also given by

$$n = 1.7 \times 10^{18} \alpha^{-1} m^{-1} \dot{m} \left(\frac{r}{r_{\rm in}} \right)^{-3/2}\ {\rm cm}^{-3}, \tag{2.2}$$

where α is the viscous parameter, $m = M/M_\odot$ and $\dot{m}$ is the mass accretion rate in units of the Eddington accretion rate $\dot{M}_{\rm Edd} = 1.4 \times 10^{17} m\ {\rm g\ s}^{-1}$. We note that the definition of the Eddington rate in Ref. 9) is ten times larger than ours.

Once temperatures, densities and drift timescales are specified, we can follow the evolution of abundance in ADAF from the outer boundary $r_{\rm out} = 100 r_g$ to $r_{\rm in}$, using a nuclear reaction network. It is likely that $r_{\rm out}$ becomes much larger during the quiescent state,[10)] but the abundance distribution is independent of the choice of larger $r_{\rm out}$, because temperature is too low to operate nuclear reactions in the outer

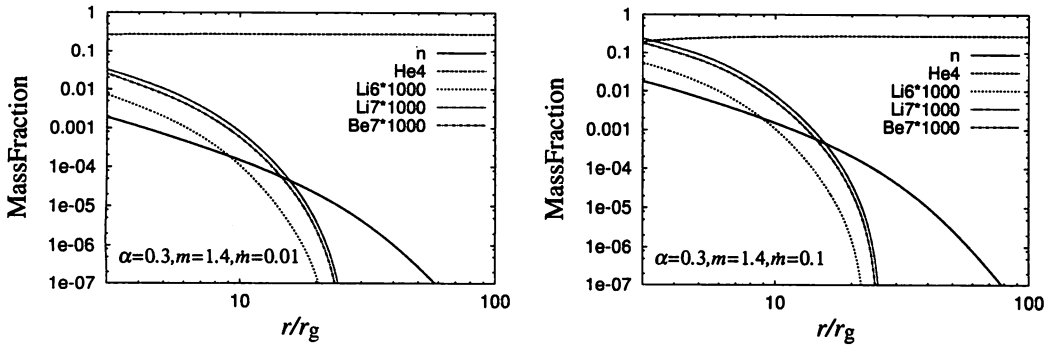

Fig. 1. Distribution of abundance in ADAF for $\alpha = 0.3$ and $m = 1.4$. The left panel indicates the case $\dot{m} = 0.01$ and the right is the case $\dot{m} = 0.1$. The solid, dashed, short-dashed, dotted and dash-dotted lines indicate the mass fractions of n, ^{4}He, ^{6}Li, ^{7}Li and ^{7}Be, respectively.

region. We have developed a nuclear reaction network with including four $\alpha - \alpha$ reactions to synthesize ^{6}He, ^{6}Li, ^{7}Li and ^{7}Be, based on a network in Ref. 5). Our network contains 21 species of nuclei; n, p, D, T, ^{3}He, ^{4}He, ^{6}He, ^{6}Li, ^{7}Li, ^{7}Be, ^{9}B, ^{11}C, ^{12}C, ^{13}N, ^{14}N, ^{15}O, ^{16}O, ^{17}F, ^{20}Ne, ^{21}Na and ^{24}Mg. It should be emphasized that photodisintegrations are not important for the abundance evolution in ADAF, since ADAF is optically thin and photons have no chance to interact with nuclei. Therefore, nuclear statistical equilibrium cannot be realized in ADAF even at high temperatures. Our network is appropriate in treating the production of n and Li, but insufficient for Be, B and heavier nuclei because of the limited numbers of nuclei and reactions. We note that ^{6}He and ^{7}Be decay to ^{6}Li and ^{7}Li with half lives of 0.806 s and 53.29 days, respectively. Initial abundances at $r_{\rm out}$ are set to be the solar composition[11] without Li.

Figure 1 shows the abundance distribution of n, ^{4}He, ^{6}Li, ^{7}Li and ^{7}Be inside ADAF for $\alpha = 0.3$ and $m = 1.4$. We set $\dot{m} = 0.01$ in the left panel and 0.1 in the right panel. Neutrons are abundant via the breakup of ^{4}He in an inner region $r < 20\, r_g$. The distribution of neutrons is similar to that in Ref. 12). Lithium is appreciably synthesized at the inner region of ADAF. Note that ^{7}Be is comparable to and slightly lower than ^{7}Li, while ^{6}He is much lower than ^{6}Li. If we adopt higher initial abundance of ^{4}He, we get higher abundance of Li, roughly proportional to the initial abundance of ^{4}He. Our Li abundance is smaller than that estimated in Ref. 3) where viscous heating rates in nuclei are proportional to their masses, so that nucleons have the same energy. Recent numerical simulations[13] show, however, that this is not the case and individual nuclei have the same energy.

§3. Li production on the secondaries

Lithium on the secondary is considered to be enhanced through the following two processes; (i) the spallation of CNO nuclei on the secondary via neutrons ejected from ADAF[4),5)] and (ii) the transportation of Li from ADAF to the secondary through the propeller effects.[3)]

3.1. *Neutron induced spallation on the secondary*

The surface of the secondary in NSSXT is bombarded by neutrons from ADAF. The equilibrium abundance of Li on the secondary is evaluated with the same manner as in BHSXT.[5] Low X-ray luminosity[14] of Cen X-4 during quiescence indicates a very low mass accretion rate $\dot{m} \leq 10^{-6}$ onto the neutron star. The number fraction of neutrons at the inner edge of ADAF is less than 2×10^{-6} for the rate. The Li abundance on the secondary is therefore $\mathrm{Li/H} \leq 10^{-12}$, which is much less than the observed abundance $(\mathrm{Li/H})_{\mathrm{obs}} \simeq 10^{-9}$. The Li enhancement via the neutron induced spallation is deficient for the observed amounts of Li on the secondary.

3.2. *Transportation of Li to the secondary through the propeller effect*

Sudden transitions in spectral states observed NSSXTs[6),15] canbe explained as the termination of mass accretion via the propeller effects. The material in ADAF is outflowed via the propeller effects, so that a fraction of Li produced in ADAF can be transfered to the secondary. Furthermore, Li on the secondary is returned to ADAF through mass accretion. We estimate an equilibrium abundance of Li. For isotropic ejection of Li from ADAF, the production rate of Li on the secondary is given by

$$\dot{M}_{\mathrm{Li}}^{+} = \dot{M} X_{\mathrm{Li,ADAF}} \left(\frac{R_*}{a}\right)^2, \tag{3.1}$$

where $X_{\mathrm{Li,ADAF}}$ is the mass fraction of Li at the ejection radius r_{ej} of ADAF, R_* is the radius of the secondary and a is the binary separation. If we take into account ^{7}Li decayed from ^{7}Be, $\dot{M}_{\mathrm{Li}}^{+}$ is doubled. The mass transfer rate of Li from the surface to ADAF is expressed as $\dot{M}_{\mathrm{Li}}^{-} = \dot{M} X_{\mathrm{Li}}$, where X_{Li} is the mass fraction of Li on the secondary. For equilibrium between the production and deposition, we set $\dot{M}_{\mathrm{Li}}^{+} = \dot{M}_{\mathrm{Li}}^{-}$. Then the equilibrium abundance is obtained to be

$$Y_{\mathrm{Li,eq}} = \frac{1}{7}\left(\frac{R_*}{a}\right)^2 X_{\mathrm{Li,ADAF}}, \tag{3.2}$$

where the average mass number of Li is set to be 7, because of larger fractions of ^{7}Li compared with ^{6}Li. We find that $Y_{\mathrm{Li,eq}}$ is comparable to $(\mathrm{Li/H})_{\mathrm{obs}}$ for $X_{\mathrm{Li,ADAF}} \simeq 10^{-7}$, which is realized at $r = 14.1 r_g$ and $18.4 r_g$ in ADAF with $\dot{m} = 0.01$ and 0.1, respectively (see Fig. 1). Note that isotopic ratio $^6\mathrm{Li}/^7\mathrm{Li} \simeq 0.19$, which is comparable to the observed ratio.[16]

The ejection radius r_{ej} is given by the Alfvén radius as

$$r_{\mathrm{ej}} = 9.74 \left(\frac{B_{\mathrm{NS}}}{10^8\mathrm{G}}\right)^{4/7} \left(\frac{m}{1.4}\right)^{-2/7} \left(\frac{\dot{m}}{0.01}\right)^{-2/7} r_g, \tag{3.3}$$

if r_{ej} is larger than the corotation radius[3]

$$r_c = 9.4 \left(\frac{m}{1.4}\right)^{1/3} \left(\frac{P_{\mathrm{NS}}}{1\,\mathrm{msec}}\right)^{2/3} \mathrm{km}, \tag{3.4}$$

otherwise the propeller effects do not work. Here B_{NS} and P_{NS} are the magnetic field and the rotational period of the neutron star, respectively. Figure 2 shows

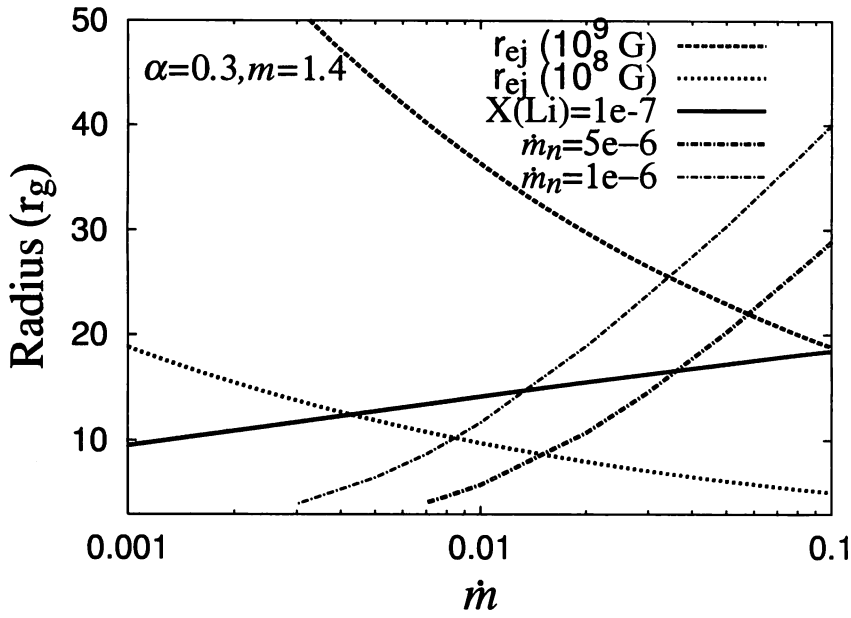

Fig. 2. Characteristic radii in ADAF as a fuction of the mass accretion rate. The solid line indicates the radius at which $X_{\rm Li} = 10^{-7}$. The dashed and the dotted lines indicate $r_{\rm ej}$ for $B_{\rm NS} = 10^8$ G and 10^9 G, respectively. The thin and the thick dash-dotted lines are the radii at which $\dot{m}_n = 1 \times 10^{-6}$ and 5×10^{-6}, respectively. Radii are measured in units of r_g.

characteristic radii as a function of $\dot{m}$. The dashed and the dotted lines indicate $r_{\rm ej}$ for $B_{\rm NS} = 10^8$ G and 10^9 G, respectively. The solid line denotes the radius at which $X_{\rm Li} = 10^{-7}$. The radius is smaller than $r_{\rm ej}$ for $B_{\rm NS} \geq 10^9$ G and $\dot{m} \leq 0.1$. Therefore, the Li enhancement via the propeller effects cannot explain the observed high Li abundance for $B_{\rm NS} \geq 10^9$ G.

The depth of an envelope exposed by Li is expressed as $(n_p \sigma_{\rm Li})^{-1}$, where n_p is the number density of protons on the surface of the secondary and $\sigma_{\rm Li}$ is the cross section for interaction between Li and protons. We simply set $\sigma_{\rm Li} = 2\sigma_T$ with the Thomson scattering cross section. The mass of the Li-exposed envelope is given by

$$M_{\rm exp,Li} \simeq 2.1 \times 10^{-11} \left(\frac{R_*}{0.7R_\odot}\right)^2 \left(\frac{0.9}{Y_p}\right) M_\odot. \tag{3.5}$$

We emphasize that the Li depletion due to convective mixing can be ignored in the Li-exposed envelope.[5] The timescale for the Li enhancement is given by

$$\begin{aligned} \tau_{\rm eq} &= 7 M_{\rm exp,Li} Y_{\rm Li,eq} / \dot{M}^+_{\rm Li} = M_{\rm exp,Li}/\dot{M} \\ &\simeq 1.1 \left(\frac{Y_p}{0.9}\right)^{-1} \left(\frac{R_*}{0.7R_\odot}\right)^2 \left(\frac{\dot{m}}{10^{-2}}\right)^{-1} \text{ yr}. \end{aligned} \tag{3.6}$$

Therefore, it takes about a year for Li to achieve the equilibrium abundance.

§4. New interpretation of soft X-ray emission in terms of neutron ADAF induced via the propeller effects

The propeller effects operating in NSSXTs during quiescence play an important role in ADAF. As shown in Fig. 1, an appreciable fraction of neutrons is produced at $r_{\rm ej}$, which is smaller than $20\,r_g$ for a reasonable set of parameters. Although almost all charged particles are ejected by magneto-centrifugal forces near $r_{\rm ej}$, neutrons are not affected by magnetic field of the neutron star. Consequently, even after the operation of the propeller effects, neutrons continues to accrete onto the neutron star. There forms *neutron ADAF* around the neutron star. Since neutrons are predominantly produced in a dense region toward the equatorial plane, neutron ADAF becomes thin compared with usual ADAF.

As neutron ADAF emits little radiation during accretion, neutrons accreting onto the neutron star liberate almost all the gravitational binding energy onto the surface of the neutron star. The liberated energy is a possible candidate for a energy budget of the blackbody-like soft X-rays. Then X-ray luminosities of 10^{32} erg s^{-1} correspond to $\dot{m}_n \sim 10^{-6}$.

We evaluate $\dot{m}_n = \dot{m} X_{n,\rm ADAF}$, where $X_{n,\rm ADAF}$ is the mass fraction of neutrons at $r_{\rm ej}$. The resulting $\dot{m}_n$ is shown in Fig. 3 as a function of $\dot{m}$ for $B_{\rm NS} = 10^8 - 10^9$ G. We find $\dot{m}_n$ is roughly proportional to $\dot{m}^3$. Using $X_{n,\rm ADAF} \propto \dot{m} r_{\rm ej}^{-3}$ from Fig. 1 and $r_{\rm ej} \propto \dot{m}^{-2/7}$ from Eq. (3.3), one obtains the same the relation.

When $B_{\rm NS}$ increases for a given $\dot{m}$, $r_{\rm ej}$ increases and thus $\dot{m}_n$ decreases. It folows that the soft X-rays of 10^{32} erg s^{-1} require $\dot{m} \geq 7 \times 10^{-3}$ for $B_{\rm NS} \geq 10^8$ G. The radii at which $\dot{m}_n = 1 \times 10^{-6}$ and 5×10^{-6} are shown in Figure 2 by the thin and thick dash-dotted lines, respectively.

§5. Comparison with observations

5.1. *Cen X-4*

Cen X-4 is an NSSXT at distance 1.2 kpc and stays in a long quiescent phase from the last outburst.[17] At the decline phase of the outburst, an X-ray burst has been observed,[18] justifying the existence of an accreting neutron star. For a mass of the secondary $M_* = 0.23 M_\odot$[16] we evaluate $R_*/a = 0.46(1 + M/M_*)^{-1/3} = 0.239$. The observed abundance[16] $({\rm Li/H})_{\rm obs} = 7.4 \times 10^{-10}$ corresponds to $Y_{\rm Li,eq} = 6.67 \times 10^{-10}(Y_p/0.9)$. We obtain $X_{\rm Li,ADAF} = 0.817 \times 10^{-7}(Y_p/0.9)$ from Eq. (3.2). The quiescent soft X-ray luminosity[19] is $L_X = 2 - 3 \times 10^{32}\,{\rm erg\,s^{-1}}$, which requires $\dot{m}_n = 1 - 2 \times 10^{-6}$. Finally we find $\dot{m} = 0.01 - 0.02$ and $B_{\rm NS} = 2 - 3 \times 10^8$ G.

It should be noted that the above accretion rate is comparable to the mass transfer rate predicted by binary evolution models[7),20] and is consistent with the average rate[21] based on an outburst luminosity and a quiescent duration.

In brief, *the scenario for the Li enhancement on the secondary in an NSSXT via the propeller effects well explain the observed high Li abundances on the secondary and the observed low blackbody-like soft X-ray luminosity, simultaneously, for reasonable values of* $\dot{m}$ *and* $B_{\rm NS}$.

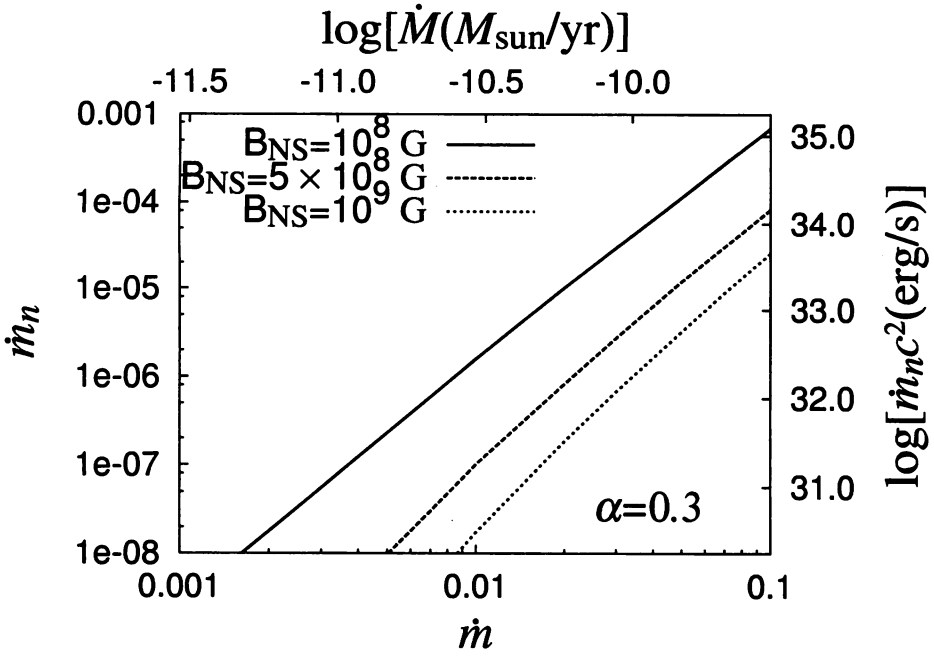

Fig. 3. Mass accretion rates of neutrons onto the neutron star through the neutron ADAF vs mass accretion rate at the outer boundary. The solid, dashed, and dotted, lines indicate $\dot{m}_n$ for $B_{\rm NS} = 10^8$G, 5×10^8G, and 10^9G, respectively.

5.2. *Aql X-1*

Aql X-1 is a typical NSSXT at 5 kpc, which shows many outbursts with irregular periods.[22] The quiescent soft X-ray luminosity[19),23)] is $L_X = 4\times10^{33}$ erg s^{-1}, which corresponds to $\dot{m}_n = 2 \times 10^{-5}$. No Li line has been detected during quiescence,[24] implying low abundance of Li on a secondary. If we set an upper limit to be 0.1 of the Li abundance of Cen X-4, we obtain $X_{\rm Li,ADAF} \leq 4 \times 10^{-9}$. The secondary mass is 0.8 $M_\odot$,[24] which leads to $R_*/a = 0.33$. Therefore we find $\dot{m} \geq 0.1$ and $B_{\rm NS} \geq 1 - 2 \times 10^9$ G.

Note that the above accretion rate is slightly larger than the mass transfer rate predicted by the binary evolution models.[7),20)]

§6. Discussion

We have fixed the viscous parameter $\alpha = 0.3$ so far. As the abundances of neutrons and Li are proportional to $\dot{m}/\alpha^2$, $\dot{m}_n$ is also proportional to $\dot{m}/\alpha^2$. Figure 4 shows the characteristic radii for $\alpha = 0.1$. Comparing with Fig. 2, we find that for lower α, the observed values Li/H and L_X require lower $\dot{m}$ but similar $B_{\rm NS}$. When $\alpha = 0.1$, we obtain $\dot{m} = 0.005 - 0.006$ and $B_{\rm NS} = 2 - 3 \times 10^8$ G for Cen X-4.

In addition to Li, protons are also transfered to the secondary from ADAF through the propeller effects. The proton-rich outflows might produce Li on the secondary via proton-induced spallation of CNO nuclei. However, protons are likely

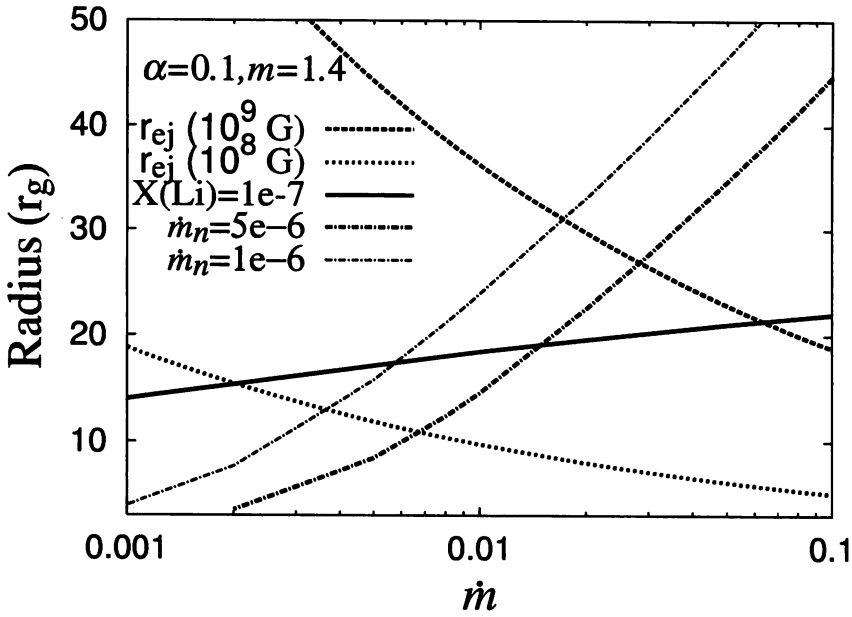

Fig. 4. Same as Fig. 2, but for $\alpha = 0.1$.

to lose their energies through the Coulomb interaction with electrons during the transportation. The timescale is estimated to be 0.0015 s at $10 r_g$ in ADAF for $\alpha = 0.3$, $m = 1.4$, $\dot{m} = 0.01$ and electron temperature 5×10^{10} K. Therefore, protons cannot participate in producing Li.

We have shown that appreciable neutrons accrete onto a neutron star even if the propeller effects turn on. A fraction of the accreted neutrons interacts with protons on the surface of the star to synthesize D and to emit γ-ray photons with 2.223 MeV. We estimate the luminosity of the γ-ray as

$$L_\gamma \simeq 4.2 \times 10^{30} \left(\frac{m}{1.4}\right) \left(\frac{\dot{m}_n}{10^{-5}}\right) \text{ erg s}^{-1}, \tag{6.1}$$

which corresponds to the photon flus 4.1×10^{-9} cm^{-2} s^{-1} at a distance of 2 kpc. This is, however, much lower than a line sensitivity of the current spectrometer.

Magnetic fields of binary radio pulsars with low-mass companions clearly correlate with the orbital periods of the binaries and the rotational period.[25] The correlation strongly suggests that the magnetic fields decay due to mass accretion in light of binary evolution model. The magnetic fields of Cen X-4 and Aql X-1 estimated in the previous section are consistent with an empirical relation between the magnetic fields and the orbital periods.[25]

§7. Summary

We have examined the Li enhancement on the surface of a secondary in a NSSXT during quiescence. Lithium is synthesized via $\alpha - \alpha$ spallation reactions in ADAF around a neutron star and is transfered to the secondary by the propeller effects. Although accretion of almost all charged nuclei and electrons in ADAF is terminated by magneto-centrifugal forces, neutrons produced in ADAF continue to accrete onto the neutron star. Accretion energy of neutrons is liberated on the surface of the star to be a possible energy budget of soft X-rays from NSSXTs. We have evaluated the mass accretion rates and magnetic fields of the neutron star from the observed values of Li abundance and soft X-ray luminosity. Our results are $\dot{M} = 2 - 4 \times 10^{-11} M_\odot$ yr^{-1} and $B_{\rm NS} = 2 - 3 \times 10^8$ G for Cen X-4, and $\dot{M} \geq 2 \times 10^{-10} M_\odot$ yr^{-1} and $B_{\rm NS} \geq 1 - 2 \times 10^9$ G for Aql X-1. Moreover, the isotopic ratio ^{6}Li/^{7}Li is found to be comparable to the observed value in Cen X-4.

We have shown that neutrons accrete onto the surface of a neutron star, and a fraction of the neutrons interact with protons to synthesize D abundantly. The residual neutrons could interact with D to produce heavier nuclei. A sequene of neutron captures might synthesize heavier neutron-rich nuclei. More importantly, accretion of neutrons possibly change the composition of the material on the surface, and could affect the duration and shape of light curves of X-ray bursts. These subjects are solved in our future works.

References

1) G. Wallerstein, Nature **356** (1992), 569.
   E. L. Martin, R. Rebolo, J. Casares and P. A. Charles, Nature **358** (1992), 129.
   E. L. Martin, R. Rebolo, J. Casares and P. A. Charles, Astrophys. J. **435** (1994), 791.
   E. L. Martin, J. Casares, P. Molaro, R. Rebolo and P. Charles, New Astron. **1** (1996), 197.
2) E. L. Martin, J. Casares, P. A. Charles and R. Rebolo, Astron. Astrophys. **303** (1995), 785.
3) I. Yi and R. Narayan, Astrophys. J. **486** (1997), 363.
4) N. Guessoum and D. Kazanas, Astrophys. J. **512** (1999), 332.
5) S. Fujimoto, R. Matsuba and K. Arai, Astrophys. J. **673** (2008), 51.
6) S. N. Zhang, W. Yu and W. Zhang, Astrophys. J. **494** (1998), L71.
7) K. Menou, A. A. Esin, R. Narayan, M. R. Garcia, J.-P. Lasota and J. E. McClintock, Astrophys. J. **520** (1999), 276.
8) M. Machida, K. Nakamura and R. Matsumoto, Publ. Astron. Soc. Japan **56** (2004), 671.
9) R. Narayan and I. Yi, Astrophys. J. **428** (1994), L13; ibid. **444** (1995), 231; ibid. **452** (1995), 710.
10) R. Narayan, D. Barret and J. E. McClintock, Astrophys. J. **482** (1997), 448.
11) E. Anders and N. Grevesse, Geochim. Cosmochim. Acta **53** (1989), 197.
12) P. Jean and N. Guessoum, Astron. Astrophys. **378** (2001), 509.
13) P. Sharma, E. Quataert, G. W. Hammett and J. M. Stone, Astrophys. J. **667** (2007), 714.
14) K. Asai, et al., Publ. Astron. Soc. Japan **48** (1996), 257.
15) S. Campana, et al., Astrophys. J. **499** (1998), L65.
    M. Gilfanov et al., Astron. Astrophys. **338** (1998), L83.
    X. Chen, S. N. Zhang and G. Q. Ding, Astrophys. J. **650** (2006), 299.
16) J. Casares et al., Astron. Astrophys. **470** (2007), 1033.
17) L. J. Kaluzienski, S. S. Holt and J. H. Swank, Astrophys. J. **241** (1980), 779.
18) M. Matsuoka, et al., Astrophys. J. **240** (1980), L137.
19) K. Asai et al., Publ. Astron. Soc. Japan **50** (1998), 611.
20) A. R. King, U. Kolb and L. Burderi, Astrophys. J. **464** (1996), L127.

21) C. O. Heinke, P. G. Jonker, R. Wijnands and R. E. Taam, Astrophys. J. **660** (2007), 1424.
22) D. Lin, R. A. Remillard and J. Homan, Astrophys. J. **667** (2007), 1073.
23) R. E. Rutledge, L. Bildsten, E. F. Brown, G. G. Pavlov and V. E. Zavlin, Astrophys. J. **559** (2001), 1054.
24) M. R. Garcia, P. J. Callanan, J. McCarthy, K. Eriksen and R. M. Hjellming, Astrophys. J. **518** (1999), 422.
25) E. P. J. van den Heuvel and O. Bitzaraki, Astron. Astrophys. 297 (1995), L41